Available online at www.sciencedirect.com
ScienceDirect
Journal of Power Sources 164 (2007) 772–781
JOURNAL OF POWER SOURCES
www.elsevier.com/locate/jpowsour

Kinetics of Ru-catalyzed sodium borohydride hydrolysis

J.S. Zhang [a], W.N. Delgass [b], T.S. Fisher [a,*], J.P. Gore [a]

[a] School of Mechanical Engineering and the Energy Center at Discovery Park, Purdue University, West Lafayette, IN 47907-2088, USA
[b] School of Chemical Engineering and the Energy Center at Discovery Park, Purdue University, West Lafayette, IN 47907-2100, USA

Received 14 August 2006; received in revised form 31 October 2006; accepted 1 November 2006
Available online 11 December 2006

Abstract

Chemical hydrides have been identified as a potential medium for on-board hydrogen storage, one of the most challenging technical barriers to the prospective transition from gasoline to hydrogen-powered vehicles. Systematic study of the feasibility of the sodium borohydride systems, and chemical-hydride systems more generally, requires detailed kinetic studies of the reaction for use in reactor modeling and system-level experiments. This work reports an experimental study of the kinetics of sodium borohydride hydrolysis with a Ru-on-carbon catalyst and a Langmuir-Hinshelwood kinetic model developed based on experimental data. The model assumes that the reaction consists of two important steps: the equilibrated adsorption of sodium borohydride on the surface of the catalyst and the reaction of the adsorbed species. The model successfully captures both the reaction's zero-order behavior at low temperatures and the first-order behavior at higher temperatures. Reaction rate constants at different temperatures are determined from the experimental data, and the activation energy is found to be 66.9 kJ mol^{-1} from an Arrhenius plot.

Keywords: Hydrogen storage; Sodium borohydride; Hydrolysis; Kinetics

1. Introduction

The prospect of peaking world-wide oil production has motivated the development of alternative energy sources and energy carriers. Hydrogen has been identified as a likely replacement energy carrier, and renewable energy sources such as solar, wind and hydro have been identified as potential drivers for future energy systems. Producing hydrogen from renewable sources and utilizing hydrogen in high-efficiency fuel cells or engines may significantly reduce greenhouse gas emissions and pollution. Furthermore, a hydrogen energy economy would be less dependent on limited fossil fuel supplies. Nevertheless, many critical technical challenges remain to be addressed before hydrogen-based energy can become widely available and economical [1].

On-board hydrogen storage has been identified as one of the most challenging technical barriers to the transition from gasoline to hydrogen-powered vehicles. Two promising hydrogen storage material categories are metal hydrides and chemical hydrides, both of which rely on catalysis to improve kinetics. The discovery of the catalytic effect of Ti compounds in the hydrogenation and dehydrogenation of sodium alanates by Bogdanovic and Schwickardi [2] has aroused increased interest in metal hydride research. The successful demonstration of Millenium Cell's sodium borohydride ($NaBH_4$) system in Daimler Chrysler's fuel cell minivan represents another potential hydrogen storage method [3]. Chemical hydride systems always involve reactions between the storage medium and a solvent, in most cases water. The reaction is generally catalyzed, and solid catalyst is preferred to facilitate recycling. To study the feasibility of sodium borohydride systems and other chemical-hydride systems systematically, detailed kinetic studies of the reaction, system-level experimental testing, and reactor modeling are essential.

Much prior catalysis research has focused on gas-phase processes primarily used in the petroleum industry. However, solid-catalyzed liquid-phase reactions, an area that has not received much attention in the past, are crucial for chemical-hydride systems. For sodium borohydride systems, the chemical hydride is premixed with water to form aqueous $NaBH_4$ solution. At room temperature, the reaction between sodium borohydride and water is very slow. To further suppress the reaction, a small amount of sodium hydroxide (NaOH) is commonly added to the $NaBH_4$ solution. Hydrogen can be liberated by contacting

* Corresponding author. Tel.: +1 765 494 5627; fax: +1 765 494 0539.
E-mail address: tsfisher@purdue.edu (T.S. Fisher).

0378-7753/$ – see front matter © 2006 Published by Elsevier B.V.
doi:10.1016/j.jpowsour.2006.11.002

Nomenclature

C_A	concentration of $NaBH_4$ at time t (kmol m^{-3})
C_{A0}	initial concentration of $NaBH_4$ (kmol m^{-3})
d	diameter of the catalyst (m)
ΔE_{act}	activation energy for the catalysis process (kJ mol^{-1})
ΔH_{ads}	heat of adsorption (kJ mol^{-1})
ΔH_{rxn}	heat of reaction (kJ mol^{-1})
k_0	zero-order rate constant (kmol s^{-1} kg catalyst^{-1})
k_1	first-order rate constant (m^3 s^{-1} kg^{-1})
k_L	rate constant for Langmuir-Hinshelwood kinetic model (kmol s^{-1} kg catalyst^{-1})
k'''_L	normalized rate constant for Langmuir-Hinshelwood kinetic model based on reactor volume (kmol m^{-3} s^{-1} kg catalyst^{-1})
k_n	nth-order rate constant (m^{3n} kmol$^{-(n-1)}$ s^{-1} kg catalyst^{-1})
k_{slope}	slope of the linear line (kmol m^{-3} s^{-1})
K	Langmuir adsorption isotherm constant (m^3 kmol^{-1})
K_0	Langmuir adsorption isotherm constant at 25 °C (m^3 kmol^{-1})
m_{cat}	weight of catalyst (mg)
R	universal gas constant (8.31 kJ kmol^{-1} K^{-1})
$\Delta S°$	entropy change of the adsorption process (kJ kmol^{-1} K^{-1})
t	time (s)
T	temperature (°C)
T_0	reference temperature, 25 °C
V	volume of the batch reactor (m^3)
V_{H_2}	the volume of H_2 collected at time t (mL)
$V_{H_2\ max}$	the total volume of H_2 collected at the end of experiment (mL)

Greek symbol

θ_A	coverage of adsorbed BH_4^- on catalyst surface

the aqueous $NaBH_4$ solution with a ruthenium (Ru) catalyst, as follows:

$$NaBH_4 + 4H_2O \xrightarrow[Ru(cat.)]{25\,^\circ C} NaB(OH)_4 + 4H_2 + Heat \quad (1)$$

The foregoing reaction is highly exothermic, with a heat of reaction of 210 kJ mol^{-1} [4]. Previous researchers have conducted preliminary studies [5–7] on its kinetics; nevertheless, these studies are predominantly qualitative. Furthermore, most previous research employed custom-made catalysts, which may not be stable and are difficult to replicate. Conversely, commercially available Ru catalysts offer good stability and consistency. Therefore, the main purpose of this paper is to quantify the kinetics of the liquid-phase reaction over a solid catalyst – sodium borohydride hydrolysis catalyzed by commercially available Ru catalyst – both to characterize the order of the reaction, and to provide a kinetic model for future reactor development. While the pH level [8,9] and other catalytic alloys [9,10] are known to affect the hydrolysis process, these factors were not considered in the present work because: (a) a pH level of 14 is the most likely for practical applications involving stabilized solutions [11], and (b) Ru remains the most common catalyst for such reactions.

2. Experimental setup

Accurate study of kinetics requires conducting experiments at constant temperature. The $NaBH_4$ hydrolysis reaction is highly exothermic; therefore, it is essential to maintain constant solution temperature by reducing the heat generation rate during experiments and by enhancing external cooling. Two methods have been used to minimize the heat generation rate during the present experiments: the use of a low concentration of $NaBH_4$, e.g. 1%, and use of a relatively small amount of catalyst to limit the reaction rate to a measurable range. Because the reaction rate increases significantly with temperature, the amount of catalyst used in the experiments was decreased for higher reaction temperatures. Type-T (copper–constantan) thermocouples with stainless steel sheaths were used to monitor solution temperature during experiments. The reaction temperature was constantly monitored and controlled by a combination of water spray cooling and water bath heating. Cooling was achieved by spraying tap water at approximately 17 °C along the neck of the flask when the solution temperature began to deviate from the desired temperature.

Fig. 1 shows the experimental setup, excluding the water spray cooling. The temperature of the water bath was maintained constant within a variation of ±0.1 °C using a thermostatic circulator. The reaction solution temperature was maintained within a variation of ±1 °C. The $NaBH_4$ solution was also premixed with 3.75% NaOH to suppress the hydrolysis reaction during storage (the PH of the solution was approximately 14). Two 25 mL flasks were used. Because of the difficulties associated with solid dispensing during gas-evolving experiments, the desired amount of ground solid catalyst in powder form was preloaded into the reaction flask together with a magnetic stirring bar. To eliminate the influence of initial wetting of the catalyst on the measured kinetics, 2 mL of de-ionized water was injected into the reaction flask to pre-wet the catalyst. The reaction flask was

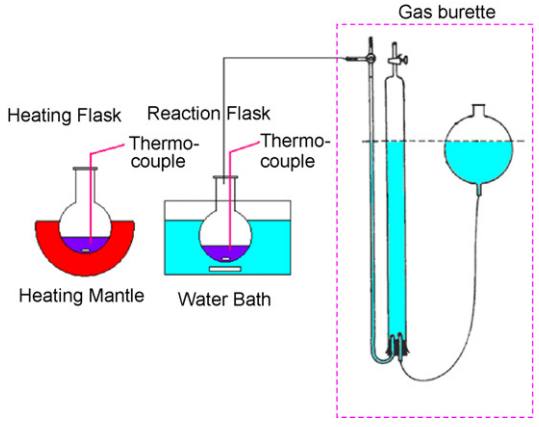

Fig. 1. Schematic of the experimental setup.

preheated by submerging it for 5 min in the water bath maintained at the desired reaction temperature. During this period the flask was stirred at 800 rpm. Then, 12 mL of 0.993% sodium borohydride aqueous solution with 3.75% sodium hydroxide as a stabilizer was injected into the heating flask. The solution was quickly heated from room temperature to several degrees above the desired reaction temperature using a small heating mantle. The purpose of the heating mantle is to minimize the heating time of the solution, which in turn minimizes the self-decomposition of the sodium borohydride aqueous solution during the heating process. In addition, using a heating mantle instead of a water bath enabled us to raise the solution temperature several degrees above the reaction temperature to account for heat losses during the process of transferring the solution from the heating flask to the reaction flask.

Approximately 8 mL reaction solution was then transferred to the other pre-heated flask by a syringe to initiate the reaction. The exact amount of solution transferred was determined by weighing the syringe before and after injection using an analytical balance. The maximum injected amount of solution was dictated by the capacity of the gas-burette, which had a measurement range of 0–250 mL. After accounting for the water used to wet the catalyst, the resulting solution's initial concentration of sodium borohydride was approximately 0.8% and the concentration of sodium hydroxide was approximately 3.0%, which is commonly used for hydrolysis purposes [5,11]. A type-T thermocouple with a stainless steel sheath was inserted into the reaction flask to monitor the reaction temperature continuously. The H_2 generated was measured in a gas burette by the volume of water it displaced.

3. Experiments

To establish a standard test procedure, a series of experiments was conducted to study the effects of catalyst support, size of catalyst particles, catalyst loading, and reactor mixing conditions before beginning kinetic measurements at different temperatures. The following section discusses the experimental results from these tests.

3.1. Effects of substrate

Three commercially available Ru catalysts from Johnson Matthey: 2 wt.% Ru on alumina pellets (3 mm in diameter and 5 mm in length, specific area ~200 $m^2 g^{-1}$), 3 wt.% Ru on carbon extrudate (2 mm in diameter and 3 mm in length, specific area ~1000 $m^2 g^{-1}$) and 0.5 wt.% Ru on carbon granules (1.7–5 mm, specific area ~1000 $m^2 g^{-1}$), were tested for stability and activity at room temperature (the constant temperature bath was not used for these three tests). The same total mass of catalyst metal of each type was used in the tests. We found that the Ru on alumina substrate broke apart severely and crumbled during the experiment. The reason could be that alumina is slightly acidic and reacts with the highly basic sodium borohydride solution because of the presence of sodium hydroxide as a stabilizer. The Ru on carbon granules also experienced significant break-up during experiments, perhaps due to the irregular shapes of the particles. In comparison, 3% Ru on carbon extrudate exhibited the highest integrity during experiments; therefore, it was used in subsequent experiments.

Table 1
Sieve set and catalyst size

Catalyst number	Mesh range	Range of catalyst size (μm)	Average catalyst size (μm)
1	#30–#40	425–600	512.5
2	#50–#60	250–300	275
3	#100–#140	106–150	128
4	#200–#230	63–75	68
5	#325–#400	38–45	41.5
6	#400–#450	32–38	35
7	#450–#500	25–32	28.5
8	#500–#635	20–25	22.5

3.2. Effects of catalyst particle sizes

To study the effect of catalyst particle size, 3% Ru on 2 mm carbon extrudate was ground and sieved into different sizes as described in Ref. [12]. The twelve different sieves were stacked on top of each other, and the average diameters of the supported catalyst particles trapped in each sieve are assumed to match the average pore sizes of the two adjacent sieves. The sieve set used and the average catalyst size in each category are listed in Table 1.

The effects of different catalyst particle sizes were studied at 25 °C and at 55 °C. Fig. 2 shows that at 25 °C, hydrogen evolution curves for 41.5 μm and 35 μm overlap each other, implying that the reaction rate did not change with a decrease of catalyst particle size from 41.5 μm to 35 μm. Fig. 3 shows similar results at 55 °C for catalyst particle sizes from 41.5 μm to 28 μm. The results indicate that the 35 μm catalyst was free from internal diffusion for temperatures from 25 °C to 55 °C, and as a result, 35 μm catalyst particles were used to study that temperature range. For temperatures from 60 °C to 85 °C, 28.5 μm catalyst particles were used to minimize internal diffusion effects. The reason that the 28.5 μm catalyst was not used from 25 °C to

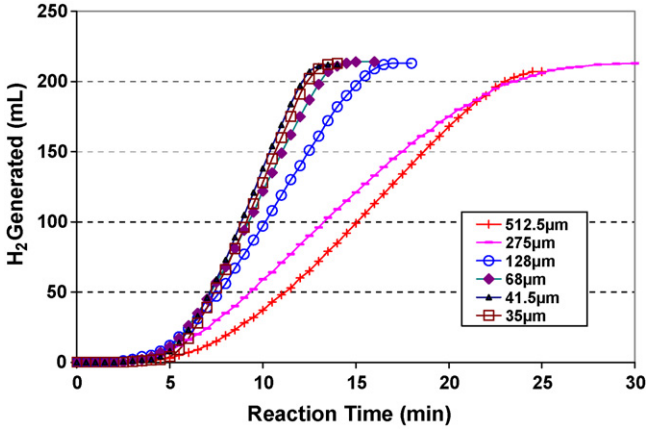

Fig. 2. Hydrogen generation as a function of time for different catalyst particle sizes (25 °C, 200 mg catalyst).

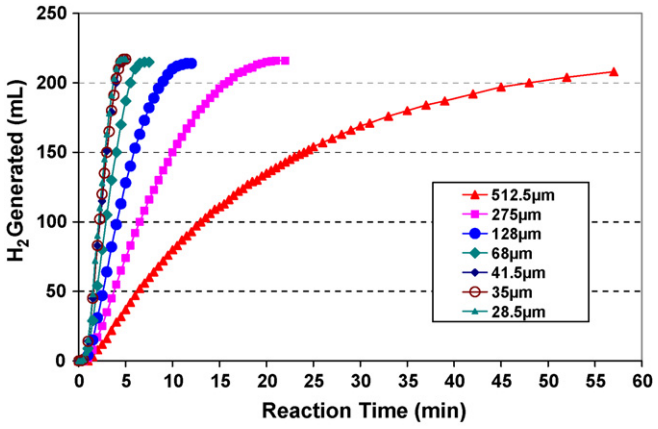

Fig. 3. Hydrogen generation as a function of time for different catalyst particle sizes (55 °C, 21.5 mg catalyst).

55 °C was the limited amount of the catalyst available from the grinding process.

3.3. Effects of stirring speed

To obtain intrinsic kinetic data independent of external diffusion effects, four tests were conducted at room temperature using four different stirring speeds, 750 rpm, 1000 rpm, 1250 rpm and 1500 rpm, and hydrogen evolution results are illustrated in Fig. 4. The curves for 750 rpm and 1500 rpm lay on top of each other, as do the curves for 1000 rpm and 1250 rpm. The small gap between these two pairs of curves is indicative of the experimental error. Therefore, the results suggest that the effect of mass diffusion across the liquid-phase boundary to the catalyst surface was eliminated when the stirring speed was at 750 rpm. For higher temperatures, liquid-phase diffusivity increases. As a result, a lower stirring speed is adequate to achieve complete mixing at higher temperatures. Therefore, the 750 rpm stirring speed is considered to be sufficient for higher temperatures as well. For all the tests reported hereafter, the stirring speed used was 1500 rpm unless otherwise stated. We note that when the solution was not stirred, the measured reaction rate was much smaller.

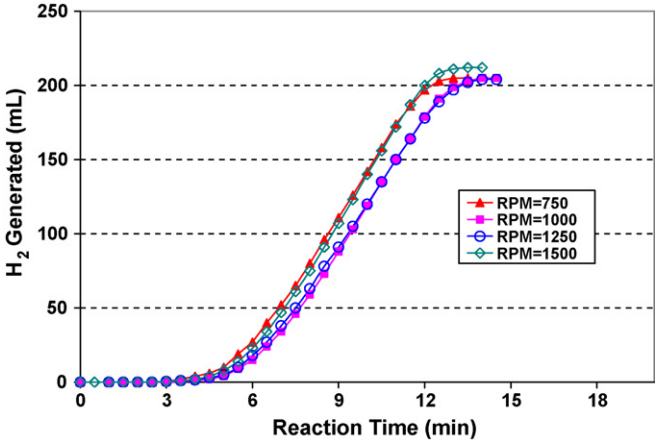

Fig. 4. Hydrogen generation as a function of time at different stirring speeds (25 °C, 200 mg, 41.5 μm size catalyst).

Table 2
Catalyst amounts used at different temperatures

Temperature (°C)	Weight (mg)	Catalyst size (μm)
25.0	200.0	35
31.1	137.6	35
34.9	87.9	35
40.7	52.7	35
45.5	34.7	35
50.9	21.8	35
56.3	21.3	35, 28.5
60.0	13	28.5
64.0	10.6	28.5
71.5	8.9	28.5
75.8	7.1	28.5
79.9	6.2	28.5
84.5	5.1	28.5

3.4. Effects of temperature

The effects of temperature were studied from 25 °C to 85 °C at intervals of approximately 5 °C. The catalyst size used from 25 °C to 55 °C was 35 μm while the catalyst size used from 60 °C to 85 °C was 28.5 μm, as explained above. Because of the increase in the reaction rate, the amount of catalyst used was reduced to a level such that the reaction process could be monitored accurately. The amounts of catalyst used in these tests are listed in Table 2.

4. Data analysis method

To analyze data from experiments conducted at different temperatures, we must convert raw data for hydrogen generation as a function of time to reaction rate versus sodium borohydride concentration or sodium borohydride concentration versus time. Assuming complete conversion of the $NaBH_4$ at the end of each experiment, the concentration at each time point based on the initial concentration, hydrogen generated, and the total hydrogen collected was calculated as follows:

$$C_A = C_{A0}\left(\frac{1 - V_{H_2}}{V_{H_2\ max}}\right) \quad (2)$$

Total hydrogen collected at the end of the experiment was also used to verify complete consumption of the borohydride. The small differences between measured and expected hydrogen production and consistency in total hydrogen generated (less than ±5% variation in asymptotic values in Figs. 2–4) over the broad parameter ranges studied serve to validate this approach. Initially a differential method was used to analyze the data in which the reaction rate was calculated based on the ratio of the difference between two successive generated hydrogen readings to the time interval [12], but the resulting reaction rate versus concentration exhibited significant scatter because of experimental errors associated with each reading. Instead, we used an integral method [13] to analyze the data. To use the integral method for batch reactor data, a kinetic model (such as zero-order, first-order and *n*th-order) must be specified. The mathematical derivations for the integration format based on four different models are given in the subsequent sections.

4.1. Zero-order kinetics

For a batch reactor with a volume V and a catalyst mass m_{cat}, the reaction rate per unit volume based on zero-order kinetics can be described as:

$$-r_A = -\frac{dC_A}{dt} = \frac{m_{cat}k_0}{V} \tag{3}$$

Note that k_0 has units of mol $(mass_{cat}\ time)^{-1}$. Integrating Eq. (3) and noting that C_A cannot be negative, we obtain:

$$C_{A0} - C_A = \frac{m_{cat}k_0}{V}t \quad \text{for } t < \frac{C_{A0}V}{m_{cat}k_0} \tag{4}$$

Therefore, a plot of $C_{A0} - C_A$ as a function of time should give a straight line, and the slope of the line can be used to calculate the zero-order rate constant k_0. In principle, the line should pass through the origin only if the reaction is zero-order during an initial period. We discuss initiation by sorption of the $NaBH_4$ on the surface of the catalyst as a possible cause of a non-zero intercept in Section 5.1.

4.2. First-order kinetics

For a batch reactor with a volume V and a catalyst mass m_{cat}, the reaction rate per unit volume based on first-order kinetics can be described as:

$$-r_A = -\frac{dC_A}{dt} = \frac{m_{cat}k_1C_A}{V} \tag{5}$$

The units of k_1 are vol $(mass_{cat}\ time)^{-1}$. Separating and integrating, we obtain:

$$-\int_{C_{A0}}^{C_A}\frac{dC_A}{C_A} = \frac{m_{cat}k_1}{V}\int_0^t dt \tag{6}$$

$$\ln\left(\frac{C_{A0}}{C_A}\right) = \frac{m_{cat}k_1}{V}t \tag{7}$$

Therefore, a plot of $\ln(C_{A0}/C_A)$ as a function of time should give a straight line, and the slope of the line can be used to calculate the first-order rate constant k_1.

4.3. nth-order kinetics

For a batch reactor with a volume V and a catalyst mass m_{cat}, the reaction rate per unit volume based on nth-order kinetics can be described as:

$$-r_A = -\frac{dC_A}{dt} = \frac{m_{cat}k_nC_A^n}{V} \tag{8}$$

The units of k_n are $vol^n\ (mol^{n-1}\ mass_{cat}\ time)^{-1}$. Separating and integrating, we obtain:

$$-\int_{C_{A0}}^{C_A}\frac{dC_A}{C_A^n} = \frac{m_{cat}k_n}{V}\int_0^t dt \tag{9}$$

$$\frac{1}{1-n}(C_{A0}^{1-n} - C_A^{1-n}) = \frac{m_{cat}k_n}{V}t \quad (n \neq 1) \tag{10}$$

Therefore, a plot of $(1/(1-n))(C_{A0}^{1-n} - C_A^{1-n})$ as a function of time should give a straight line through the origin, and the slope of the line can be used to calculate nth-order rate constant k_n.

4.4. Langmuir-Hinshelwood Model

The reaction studied here involves a liquid phase reaction on a catalyst surface. We assume that the reaction consists of two important steps. The first step is the equilibrated adsorption of BH_4^- on the surface of the catalyst as shown in the following equation:

$$BH_4^- + * \rightleftharpoons BH_4^-\cdot * \tag{11}$$

The surface coverage θ_A of adsorbed species is given by the Langmuir adsorption isotherm [14]:

$$\theta_A = \frac{KC_A}{1 + KC_A} \tag{12}$$

The second step is the reaction of the adsorbed species to form hydrogen as:

$$BH_4^-\cdot * + 2H_2O \rightarrow BO_2^-\cdot * + 4H_2\cdot * \tag{13}$$

Because water is abundant, the reaction is assumed to be proportional to the quantity of adsorbed $NaBH_4$ molecules θ_A. Then, for a reactor with a volume V and a catalyst mass m_{cat}, the reaction rate per unit volume can be described as:

$$-r_A = \frac{m_{cat}k_L\theta_A}{V} \tag{14}$$

Here, k_L has units mol $(mass_{cat}\ time)^{-1}$. Combining Eqs. (12) and (14):

$$-r_A = -\frac{dC_A}{dt} = \frac{m_{cat}}{V}k_L\frac{KC_A}{1 + KC_A} \tag{15}$$

Eq. (15), representing the combination of Langmuir adsorption isotherm and kinetics that are first-order in the adsorbed species, is called the Langmuir-Hinshelwood kinetic model [14].

The adsorption coefficient K normally varies with temperature according to:

$$K = A\exp\left(-\frac{\Delta H_{ads}}{RT}\right) \tag{16}$$

That is, K decreases with increasing temperature because the enthalpy of adsorption is almost always negative. As a result, at sufficiently high temperatures, KC_A is much less than unity and the reaction kinetics shown in Eq. (15) become first-order. At lower temperatures, K becomes larger. As a result KC_A is much greater than unity, and the reaction kinetics shown in Eq. (15) become zero-order. To facilitate data analysis, Eq. (16) can also be written as:

$$K = K_0\exp\left(\frac{\Delta H_{ads}}{RT_0} - \frac{\Delta H_{ads}}{RT}\right) \tag{17}$$

Separating and integrating Eq. (15), we obtain:

$$-\int_{C_{A0}}^{C_A}\frac{1 + KC_A}{KC_A}dC_A = \int_0^t \frac{k_Lm_{cat}}{V}dt \tag{18}$$

$$(C_{A0} - C_A) + \frac{1}{K}\ln\left(\frac{C_{A0}}{C_A}\right) = \frac{k_L m_{cat}}{V} t \quad (19)$$

Plotting $(C_{A0} - C_A) + (1/K)\ln(C_{A0}/C_A)$ as a function of time should give a straight line, and the slope of the line (k_{slope}) can be used to calculate k_L as follows:

$$k_{slope} = \frac{k_L m_{cat}}{V} \quad (20)$$

We note that the left side of Eq. (19) contains the left side of Eq. (4) of the zero-order model, the left side of Eq. (7) of the first-order model, and the adsorption coefficient K. Therefore, this model can be considered to be a combination of zero-order and first-order models, with the adsorption coefficient K determining which term is more important. The use of the adsorption coefficient K enables the model to capture zero-order behavior at low temperatures and first-order behavior at high temperatures. Note, however, that the value of K must be assumed in order to prepare the linear plot implied by Eq. (19).

Because the volume of the batch reactor was always 10 mL, a normalized reaction rate constant $k_L''' = (k_L/V) = (k_{slope}/m_{cat})$ was used to simplify data analysis.

4.5. Application of the kinetic models

Because an initial lag in the reaction consistently occurred, some data were neglected in curve-fitting the linearized models. At the end of most experiments, the reaction began to deviate from zero-order kinetics because of the limited reactant available, and some of the data at the end of the experiments were also excluded. In the analysis, we first tried both zero-order and first-order models to fit the data, but neither of them applied well to the whole temperature range from 25 °C to 85 °C. The nth-order model fit data from 25 °C to 85 °C fairly well but required the reaction order to increase with temperature. These results led us to the Langmuir-Hinshelwood model as a means to fit the kinetic behavior over the full temperature range.

To use Eqs. (19) and (16) in fitting the experimental data, two variables in Eq. (17) must be estimated first. K_0 was determined by manually fitting the data at 25 °C where $T = T_0$ with a wide range of K_0 values. Through visual observation, we found that only values near $K_0 = 0.22\,L\,mmol^{-1}$ matched the linearity of the data, as shown in Fig. 5. The uncertainty range for K_0 is from $0.12\,L\,mmol^{-1}$ to $0.50\,L\,mmol^{-1}$, i.e. this range of K_0 values preserves the linearity. As also shown in Fig. 5, values of $K = 0.05\,L\,mmol^{-1}$ and $K = 1\,L\,mmol^{-1}$ give unacceptable fits. The enthalpy of adsorption was determined similarly by manually fitting the 85 °C data. It was found that $\Delta H_{ads} = -35\,kJ\,mol^{-1}$ produced a good fit to the linear portion of the data, as shown in Fig. 5. The range of reasonable values for ΔH_{ads} is from $-30\,kJ\,mol^{-1}$ to $-40\,kJ\,mol^{-1}$, and Fig. 5 shows that the fits with $\Delta H_{ads} = -20\,kJ\,mol^{-1}$ or $-60\,kJ\,mol^{-1}$ are clearly unacceptable. With the assumed K_0 and ΔH_{ads} values, the Langmuir model fits the data at 55 °C very well, as also shown in Fig. 5.

To evaluate the validity of K_0 and ΔH_{ads} obtained above, we turn to adsorption theory. The adsorption coefficient can be related to the entropy change and the heat of adsorption as [15]:

$$\begin{aligned} K &= \exp\left(\frac{\Delta S^\circ}{R} - \frac{\Delta H_{ads}}{RT}\right) = K_0 \exp\left(\frac{\Delta H_{ads}}{RT_0} - \frac{\Delta H_{ads}}{RT}\right) \\ &= 0.22 \exp\left(\frac{-35 \times 10^3}{8.31 \times 298}\right) \exp\left(-\frac{\Delta H_{ads}}{RT}\right) \\ &= \exp\left(\frac{-15.6 \times 8.31}{R} - \frac{\Delta H_{ads}}{RT}\right) \\ &= \exp\left(\frac{-130.0}{R} - \frac{\Delta H_{ads}}{RT}\right) \end{aligned} \quad (21)$$

Therefore:

$$\Delta S^\circ = -130\,kJ\,kmol^{-1}\,K^{-1} \quad (22)$$

The fact that $\Delta S^\circ < 0$ indicates that the total disorder in the system decreases in the adsorption process, and is thus consistent with expectations.

4.6. Validation of data analysis method

To compare the reaction rates from two different tests with different amounts of catalyst, the slope obtained in Fig. 5 was normalized by the amount of catalyst used to obtain normalized reaction rate constant, k_L'''. To verify the validity of this method, two tests using different amounts of catalyst were conducted at room temperature. One used 150 mg of catalyst while the other used 200 mg of catalyst. The difference between the measured k_L''' values is within 3%, further supporting the validity of the data analysis method used in this work.

5. Results and discussion

5.1. Adsorption of reactant on the catalyst surface

At lower temperatures, the time needed for the initial H_2 bubble to appear was much longer than that at higher temperatures. In the curve fitting, these initial data points were ignored.

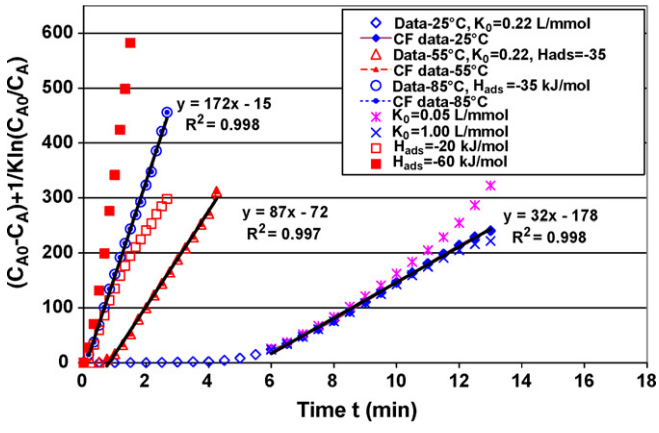

Fig. 5. Data analysis based on Langmuir-Hinshelwood model. CF data means data used in curve-fitting process, ignoring the initial data points.

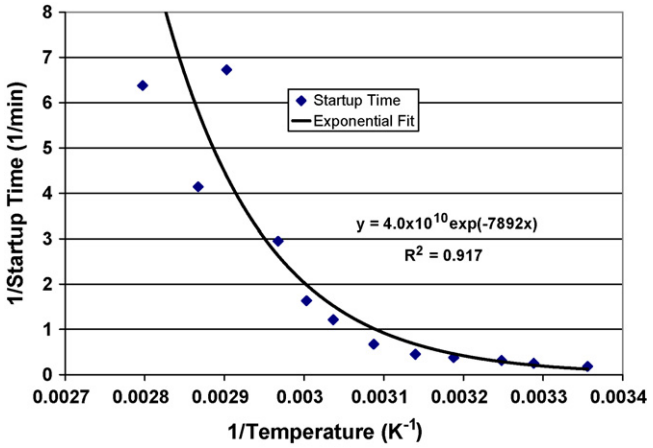

Fig. 6. The inverse of startup time as a function of the inverse of temperature.

We assume that this initial period occurred because the catalyst surface had not yet reached the adsorption equilibrium that is assumed in the Langmuir-Hinshelwood model discussed above. We can calculate the induction or sorption time by extrapolating the linear fit to its intercept with the time axis. The inverse of the sorption time is related to the sorption rate. The resulting estimates of the sorption rates are plotted in Fig. 6. It is interesting to note that this measure of the sorption rate varies exponentially with inverse temperature, which is expected Arrhenius behavior.

5.2. Effects of stirring speed

The experimental data in Fig. 4 were analyzed using the Langmuir-Hinshelwood model, and results are compiled in Table 3. The normalized reaction rates match the theory well, within ±3%, indicating that external diffusion effects were insignificant when stirring speed varied from 750 rpm to 1500 rpm. This result also validates the conclusions in Section 3.3.

5.3. Effects of catalyst size

The Langmuir-Hinshelwood model was used to analyze data in Figs. 2 and 3, and the results are compiled in Tables 4 and 5. At 25 °C, the normalized reaction rate constant k_L''' in general increased with decreasing catalyst size, doubling as the catalyst size decreased from 512.5 μm to 35 μm. At 55 °C, the normalized reaction rate constant k_L''' also increased with decreasing catalyst size as expected because the true rate constant generally increases faster with temperature than the effective diffusivity, thereby causing the effectiveness factor to decrease at a given particle size and the effect of particle size to be more marked at higher temperatures. The effective value of k_L''' increased almost 20-fold when the catalyst size decreased from 512.5 μm to 35 μm for reactions at 55 °C. The small variation in effective k_L''' for catalyst diameters of 28.5–41.5 μm suggests that the rate is independent of particle size in this range.

5.4. Effects of temperature and activation energy

Experimental data at different temperatures ranging from 25 °C to 85 °C were analyzed using the Langmuir-Hinshelwood model, and the results appear in Table 6. All correlation coefficients were larger than 0.99, implying the Langmuir-Hinshelwood model captures the reaction process at different temperatures very well. We note that normalized reaction rate constant, k_L''', increased more than 130-fold when the temperature increased from 25 °C to 85 °C.

The reaction rate constant, k_L''', at different temperatures can be plotted on an Arrhenius plot to calculate the activation energy of the catalyzed reaction as shown in Fig. 7. A good fit occurs with a correlation coefficient of 0.975, supporting the assumption that the 28.5 μm catalyst size is sufficient to avoid significant diffusion influences in the 55–85 °C temperature range. We note, however, that a careful examination of Fig. 7 reveals that the initial slope of the curve is higher than that of the later part of the curve, perhaps due to the onset of diffusion effects at higher temperatures or to experimental error. The high-temperature data exhibit significant scatter because of errors associated with temperature control and measurement of the small weight of catalyst used to accommodate the higher activity. Taking data only from 25 °C to 55 °C, we calculate the upper bound of the activation energy to be 83.5 kJ mol^{-1}, which is about 20% higher than the calculated value of 66.9 kJ mol^{-1} based on data from 25 °C to 85 °C.

From Fig. 7, the relation between the normalized reaction rate and temperature can be written as:

$$k_L''' \ (\text{mmol L}^{-1}\,\text{min}^{-1}\,\text{mg cat.}^{-1}) = \exp\left(-\frac{8054.6}{T_K} + 25.601\right) \quad (23)$$

The above equation can be used to calculate the rate constant k_L and to convert it to standard units as:

$$k_L \ (\text{kmol s}^{-1}\,\text{kg cat.}^{-1}) = \exp(16.903)\exp\left(-\frac{8054.6}{T_K}\right) \quad (24)$$

Eqs. (15), (17) and (24) represent the final form of the present kinetic model developed for reactor design and modeling.

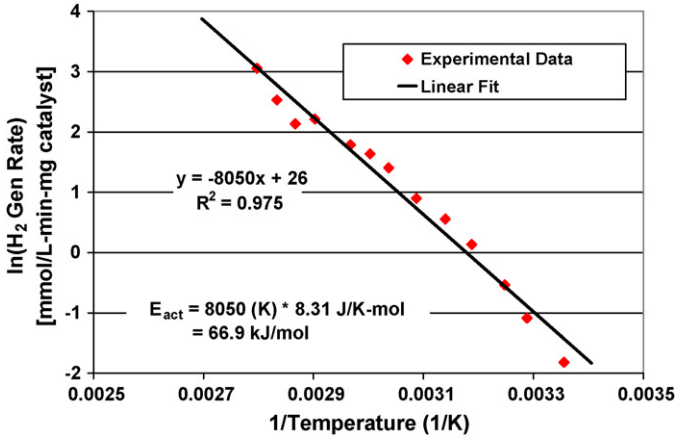

Fig. 7. Arrhenius plot for sodium borohydride hydrolysis on ruthenium catalyst.

Table 3
Effects of stirring speed on k_L''' (25 °C)

Stirring speed (rpm)	Weight (mg)	Rate equations[a] [y (mmol L^{-1}), x (min)]	Correlation coefficient, R^2	k_L''' (mmol L^{-1} min^{-1} mg^{-1})
750	200.1	$y = 30.3x - 155$	0.997	0.151
1000	198.6	$y = 30.0x - 175$	0.998	0.151
1250	200.1	$y = 29.7x - 170$	0.999	0.148
1500	199.4	$y = 30.9x - 168$	0.998	0.155

[a] Equation $y = ax + b$ comes from linear fitting of the experimental data based on Eq. (19). K in Eq. (19) was calculated based on Eq. (17). The non-zero intercept b is due to the initiation process explained in Section 5.1. The slope a is equal to $k_L m_{cat}/V$ based on Eq. (20).

Table 4
Effects of different catalyst particle sizes on k_L''' (25 °C)

Catalyst size (μm)	Weight (mg)	Rate equations[a] (mmol L^{-1} vs. min)	Correlation coefficient, R^2	k_L''' (mmol L^{-1} min^{-1} mg^{-1})
512.5	200.3	$y = 14.3x - 106$	0.999	0.071
275	199.3	$y = 12.6x - 63.8$	0.999	0.063
128	199.5	$y = 21.5x - 110$	0.999	0.108
68	199.3	$y = 26.9x - 140$	0.997	0.135
68	199.5	$y = 27.9x - 147$	0.999	0.140
41.5	199.4	$y = 32.5x - 178$	0.998	0.162
35	199.6	$y = 31.6x - 179$	0.997	0.158

[a] Refer to the note in Table 3.

Table 5
Effects of different catalyst particle sizes on k_L''' (55 °C)

Catalyst size (μm)	Weight (mg)	Rate equations[a] (mmol L^{-1} vs. min)	Correlation coefficient, R^2	k_L''' (mmol L^{-1} min^{-1} mg^{-1})
512.5	21.2	$y = 4.4x + 46$	0.906	0.206
275	21.5	$y = 15.5x + 5$	0.989	0.723
128	21	$y = 30.4x - 16$	0.993	1.447
68	21.3	$y = 54.7x - 48$	0.999	2.568
41.5	21.5	$y = 79.3x - 68$	0.999	3.688
35	21.3	$y = 80.1x - 68$	0.999	3.759
28.5	21.3	$y = 86.9x - 72$	0.997	4.078

[a] Refer to the note in Table 3.

Table 6
Effects of temperature

Temperature (°C)	Weight[a] (mg)	Rate equations[b] (mmol L^{-1} vs. min)	Correlation coefficient, R^2	k_L''' (mmol L^{-1} min^{-1} mg^{-1})
25.0	200	$y = 32.5x - 178$	0.998	0.162
31.1	137.6	$y = 46.5x - 184$	0.999	0.338
34.9	87.9	$y = 51.4x - 165$	0.999	0.585
40.7	52.7	$y = 60.4x - 160$	0.998	1.147
45.5	34.7	$y = 60.5x - 134$	0.999	1.745
50.9	21.8	$y = 53.6x - 80$	0.999	2.461
56.3	21.3	$y = 86.9x - 72$	0.997	4.078
60.0	13	$y = 66.9x - 41$	0.998	5.146
64.0	10.6	$y = 63.2x - 21$	0.998	5.966
71.5	8.9	$y = 81.5x - 12$	0.997	9.157
75.8	7.1	$y = 60.1x + 15$	0.994	8.461
79.9	6.2	$y = 78.0x + 4$	0.993	12.573
84.5	5.1	$y = 109x - 17$	0.998	21.274

[a] Refer to Table 2 on the information of catalyst size.
[b] Refer to the note in Table 3.

Table 7
Effects of different catalyst loading[a,b]

Catalyst loading	Weight (mg)	Rate equations[c] (mmol L^{-1} vs. min)	Correlation coefficient, R^2	k_L''' (mmol L^{-1} min^{-1} mg^{-1})
3%	199.4	$y = 32.5x - 178$	0.998	0.163
4.41%	136.0	$y = 67.2x - 223$	0.995	0.336
10%	59.8	$y = 107x - 254$	0.997	0.539
5% wet	238.9	$y = 157x - 168$	0.996	0.789

[a] The sizes of all catalysts were 41.5 μm except for 5% wet, whose size was not available because the catalyst all clusters together due to water.
[b] k_L''' was calculated based on the equivalent weight of 3% Ru on carbon to facilitate comparison between different catalyst.
[c] Refer to the note in Table 3.

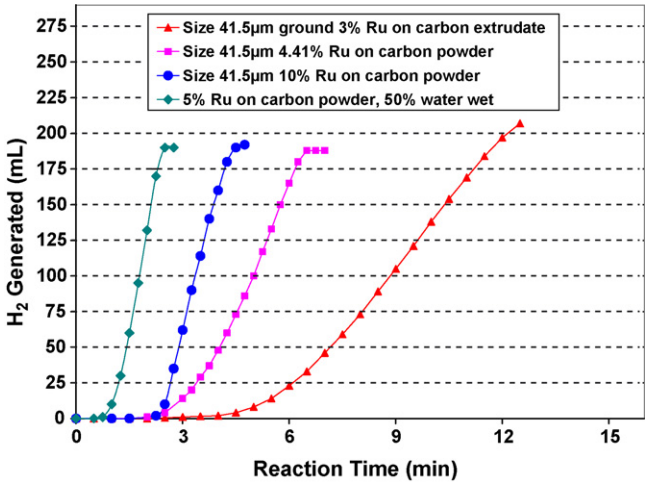

Fig. 8. Hydrogen generation as a function of time for different catalyst loadings (25 °C, 6.0 mg net Ru).

5.5. Effects of different catalyst loadings

To study the influence of the catalyst loading, four tests were conducted at room temperature. The first test used ground 3% Ru on carbon extrudate. The second test used 4.41% Ru on activated carbon powder, while the third used 10% Ru on activated carbon powder. The last test used 5% Ru on activated carbon powder, nominally 50% water wet (i.e. the final catalyst contains 50% of water by weight). The net amount of Ru in each test was maintained constant, and the size of catalyst used was 41.5 μm except for the 5% catalyst, whose size was not available because the catalyst particles clustered together. Fig. 8 shows hydrogen generation as a function of time for different catalyst loadings, and Table 7 contains the results of the analysis. In principle, the differences in observed rates could derive from the highly exothermic nature of the reaction, but the spread of k_L''' by a factor of 4.8 would require a temperature rise of approximately 18 °C, which is unlikely considering the small catalyst particle size and the liquid medium available for heat transfer. The variations in rate imply that the weight of Ru alone is not sufficient to characterize the catalysts. Ru particle size, Ru distribution on the particle surface as opposed to within the volume, and the influence of the carbon surface hydrophobicity on accessibility of the pore structure to the reacting liquid are some of the properties could all differentiate the catalysts. The differences in catalytic efficiency of the Ru, shown in Fig. 8 and Table 7, indicate that further optimization of the process may be possible and that more detailed catalyst characterization is warranted in future work.

6. Conclusions

A detailed kinetic study of sodium borohydride hydrolysis on Ru-on-carbon catalyst has been conducted. Experimental data show zero-order kinetic behavior at low temperatures and first-order kinetic behavior at high temperatures. Based on experimental observations, a unified kinetic model was developed. The results indicate that the reaction consists of two important steps: the adsorption of sodium borohydride on the surface of the catalyst and the reaction of the adsorbed species on the catalyst surface. These steps are combined in the classical Langmuir-Hinshelwood model that shows that the adsorption step is responsible for variation of kinetic order of the reaction from low to high temperatures. Furthermore, reaction rate constants at different temperatures were determined from experimental data, and the activation energy of the catalyzed process was determined from an Arrhenius plot.

Acknowledgement

The primary author thanks Prof. P.V. Ramachandran in Purdue's Department of Chemistry for the access to the facilities of the Herbert C. Brown Center for Borane Research.

References

[1] U.S. Department of Energy, Office of Basic Energy Sciences, Basic research needs for the hydrogen economy, report available at: http://www.sc.doe.gov/bes/hydrogen.pdf, 2003.
[2] B. Bogdanovic, M. Schwickardi, J. Alloys Compd. 253–254 (1997) 1–9.
[3] J. Hyde, Chrysler offers fuel cell van with soapy twist. Reuters World Environment News, 12 December 2001, http://www.planetark.org/dailynewsstory.cfm/newsid/13671/story.htm.
[4] J.S. Zhang, D. Hazra, T.S. Fisher, P.V. Ramachandran, J.P. Gore, Int. J. Hydrogen Energy 31 (2006) 2292–2298.
[5] S.C. Amendola, S.L. Sharp-Goldman, M.S. Janjua, M.T. Kelly, P.J. Petillo, M. Binder, J. Power Sources 85 (2000) 186–189.
[6] S.C. Amendola, S.L. Sharp-Goldman, M.S. Janjua, N.C. Spencer, M.T. Kelly, P.J. Petillo, M. Binder, Int. J. Hydrogen Energy 25 (2000) 969–975.
[7] S.U. Jeong, R.K. Kim, E.A. Cho, H.-J. Kim, S.-W. Nam, I.-H. Oh, S.-A. Hong, S.H. Kim, J. Power Sources 144 (2005) 129–134.
[8] H.I. Schlesinger, H.C. Brown, A.E. Finholt, J.R. Gilbreath, H.R. Hoekstra, E.K. Hyde, J. Am. Chem. Soc. 75 (1953) 215–219.
[9] C.M. Kaufman, B. Sen, J. Chem. Soc., Dalton Trans. (1985) 307–313.

[10] H.C. Brown, C.A. Brown, J. Am. Chem. Soc. 84 (1962) 1493–1494.
[11] Q. Zhang, G. Smith, Y. Wu, R. Mohring, Int. J. Hydrogen Energy 31 (2006) 961–965.
[12] G.F. Froment, K.B. Bischoff, Chemical Reactor Analysis and Design, John Wiley & Sons, New York, 1990 (chapter 3).
[13] H.S. Fogler, Elements of Chemical Reaction Engineering, Prentice Hall PTR, New Jersey, 1999.
[14] C.N. Satterfield, Heterogeneous Catalysis in Practice, McGraw-Hill Book Company, New York, 2000.
[15] J. Tóth, Adsorption: Theory, Modeling, and Analysis, Marcel Dekker, New York, 2002.